Journal of Engineering and Technological Advances (JETA)
https://jeta.segi.edu.my/index.php/segi
2025 Vol. 10 No. 2

INNOVATIVE DESIGN OF BIODEGRADABLE STENTS: ENHANCING DURABILITY AND COMPATIBILITY TO MITIGATE RESTENOSIS AND THROMBOSIS IN VASCULAR TREATMENTS

[1]Morad, S. *, [1]Shariq, M.

[1] School of Architecture, Computing and Engineering, Department of Engineering, The University of East London, London, E16 2RD, UK.

* Corresponding Author: s.morad@uel.ac.uk TEL: (+44) 20 8223 2353

Received: 4 November 2025; Accepted: 17 November 2025; Published: 31 December 2025

doi: 10.35934/segi.v10i2.160

Highlights:

- This study aims to create a stent that minimizes vein blockages and enhances durability.
- Stent model designed using SolidWorks and three simulations conducted.
- Device achieve high radial strength, addressing restenosis, thrombosis, and mechanical durability.

Abstract: Heart diseases are the leading global causes of mortality and morbidity due to obstructed blood vessels. Current clinical practice primarily utilizes stents, but standard models encounter significant limitations, including restenosis, thrombosis, mechanical failure, and issues pertaining to performance and biometric longevity. This research aims to create a novel arterial stent that effectively minimizes vein blockages while enhancing durability and compatibility. with biological environments. The study employs advanced methodologies such as finite element analysis (FEA) and computational fluid dynamics (CFD) simulations to rigorously assess and optimize stent geometry and material characteristics. Key considerations include mechanical stability, decreased restenosis rates, and the potential for controlled degradation using biodegradable materials like magnesium alloys and polymer-metal composites. A magnesium alloy stent model was designed using SolidWorks, followed by three tiers of simulations. After simulating one million cardiac cycles, the stent exhibited fatigue-resilient behaviour in both dynamic linear and nonlinear analyses. The collective results of the simulations affirm that the device achieves high radial strength (~550 N mm^{-1}), while also offering compliant expansion and effective addressing of the issues surrounding restenosis, thrombosis, and mechanical durability. This innovative approach has the potential to reshape clinical practices, enhance patient outcomes, and establish a benchmark for future stent design research. Future work is suggested to diffuse local stress peaks, alongside outlining a roadmap for transitioning from in vitro and in vivo studies to regulatory approval and subsequent clinical application.

Keywords: Stents; Computational fluid dynamics (CFD); Finite element analysis (FEA); Magnesium alloy; Balloon expansion analysis.

1. Introduction

Cardiovascular diseases (CVD) are the leading cause of death worldwide and place a significant strain on healthcare systems. The World Health Organization (WHO) reports that every year, CVDs account for 17.9 million deaths, accounting for approximately 32% of deaths across the world. The most common underlying problem that can lead to CVDs is atherosclerosis which causes lipids, cholesterol and waste particles to build up in the arteries, narrowing them and increasing the risk of heart attack and stroke (Libby, 2021). Given the increasing societal and economic burden of these diseases, effective diagnostic and intervention methods are key to improving public health and reducing the burden on healthcare systems (Benjamin et al., 2019).

Today, cardiologists depend on stent implantation, primarily for patients with blocked arteries such as coronary artery disease (CAD) and peripheral artery disease (PAD). During angioplasty, stents are deployed to restore the patency of arteries, improve blood circulation and prevent the arteries from narrowing again (Gierig et al., 2024). Even though stents have been confirmed to be effective, they are still associated with risks such as in-stent restenosis, stent thrombosis and insufficient biocompatibility (Nicolas et al., 2023). Therefore, experts must keep researching stents to address their mechanical and biological limitations (Andreou et al., 2020).

Cardiovascular stents undergone significant evolution since they were first introduced. The introduction of balloon-expandable metal stent (Palmaz, 1986) significantly reduced acute vessel closures after angioplasty and paved the way for the development of bare-metal stents (BMS). Subsequent clinical evaluation, however, revealed that BMS placement often caused neointimal hyperplasia, an injury-related buildup in the arterial lining, leading to in-stent restenosis in 20–30% of the patients six months after the procedure (Lüscher et al., 2007; Stefanini and Holmes, 2013; Iqbal et al., 2013). Despite advances in stent strut strength, radial performance and strut thickness, BMS reached a fundamental biological limit (Zhang et al., 2022). To decrease trauma and reduce obstructions, ultrathin stents (<80 μm) were introduced, which improved outcomes but proved ineffective in cases of severe arterial disease (Nicolas et al., 2023).

As a result of the anti-proliferative drugs incorporated into their polymeric coatings, drug-eluting stents (DES) emerged as a major advancement over BMS in addressing restenosis (Tijssen et al., 2017). While DES successfully decreased restenosis rates, they also delayed endothelial healing and increased the risk of late stent thrombosis (Garg and Surrey, 2010). This highlighted a fundamental trade-off: effectively suppressing tissue growth also impaired the vessel's natural healing process (Morice et al., 2002; Finn et al., 2007). Ultimately, the polymer coatings and stainless-steel platforms that enabled controlled drug release were themselves found to cause chronic inflammation and damage to the vascular tissue (Joner et al., 2006).

Bioabsorbable stents (BAS) offer a promising therapeutic approach (Tenekecioglu et al., 2017), but they face challenges, including chronic complications and incomplete resorption after arterial healing. Current materials like polylactic acid (PLA) often lack sufficient radial strength under cyclic mechanical loading, which is common in coronary arteries (Tamai et al., 2000). Several bioabsorbable scaffolds have been developed using polymers like PLA or PGA; however, their limited strength and thick struts often result in high stiffness, making them challenging to deliver through the vasculature (Gao et al., 2020). These polymeric BAS often face a trade-off, exhibiting both insufficient strength and brittleness. Therefore, enhancing their mechanical strength and controlling their degradation profile are key to improving their clinical performance (Ghafari et al., 2023).

Magnesium-based stents are gaining interest due to their mechanical integrity and favourable biocompatibility, making them suitable for temporary coronary artery stents (Waksman et al., 2013). However, rapid biodegradation rates necessitate careful control to maintain vessel support during the healing phase (Kumar et al., 2025). Next-generation Mg alloys now exhibit sufficient radial strength for clinical use and feature controllable corrosion profiles (Aikin et al., 2024). Materials engineering plays a crucial role in controlling magnesium corrosion, with methods like anodization, micro-arc oxidation (MAO), fluoride conversion coatings, and polymeric drug layers being used to control corrosion and promote endothelialisation (Amukarimi and Mozafari, 2021). Furthermore, computational modelling and finite element analysis have been used to optimize strut thickness and cell patterns, minimizing stress shielding and reducing flow disturbances (Chen et al., 2024).

Despite technological advancements, current stent designs continue to face significant challenges. Inadequate radial strength and flexibility can cause uneven vessel expansion, increasing restenosis risk (Byrne et al., 2015). Stent thrombosis, late endothelialisation, and

inflammatory responses lead to life-threatening complications (Finn et al., 2007). Chronic inflammation and hypersensitivity resulting from adverse material-tissue interactions also pose significant challenges (Antonini et al., 2023). Furthermore, mechanical failure, including fractures and deformations, compromises long-term functionality (Tamai et al., 2000; Ormiston and Serruys, 2009).

This study addresses key limitations in current stent technologies through the design and validation of a novel arterial stent, targeting reduced restenosis and thrombosis, improved mechanical performance, and enhanced biocompatibility using advanced design and materials engineering informed by FEA and CFD analyses.

2. Materials and Methods

2.1. Stent Design

Most conventional stents are structured with ring or diamond shapes; however, this design employs a racetrack-shaped cell to reduce stress concentrations and allow the vessel to adapt to the stent (**Figure *1***).

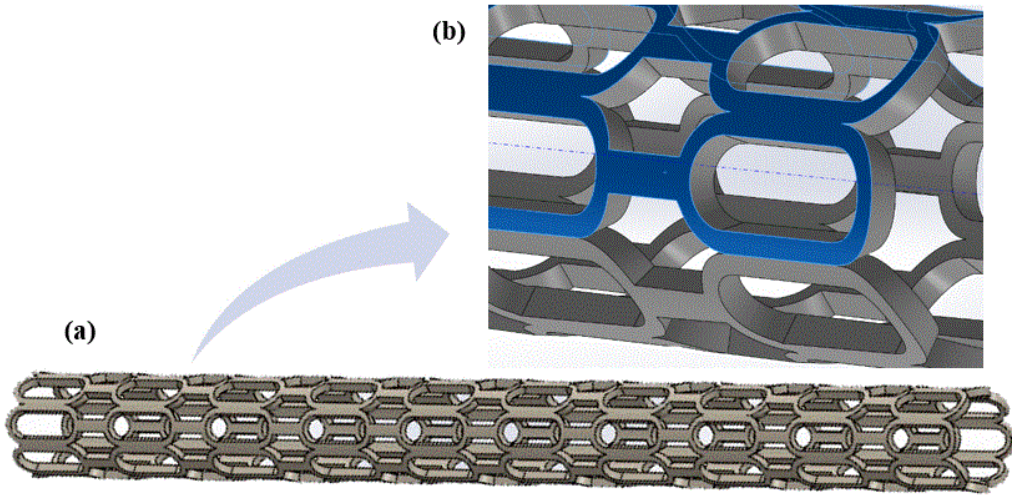

Figure 1. Stent design. (a) full length of the stent, (b) an enlarged part of the stent showing a detailed racetrack-shaped cell.

The strut geometry was optimized based on findings from simulations, anatomical knowledge, and manufacturing constraints. Key parameters and structural dimensions of the stent are summarized **Table *1***.

Table 1. Summary of key parameters used in the design of the stent.

Parameter	Description/Value
Stent type	Balloon-expandable racetrack cell
Material	Magnesium alloy
Stent length	30 mm (customizable)
Outer diameter (non-expanded)	1.6 mm
Outer diameter (expanded)	3.5 mm
Foreshortening	5% (Minimal length reduction)
Radial recoil	<5.2% (Controlled elasticity)
Radial strength	>550 N/mm
Structural Dimensions	**Value (rationale)**
Thickness	0.07 mm (ideal flexibility and stability)
Width	0.12 mm (for optimal stress support)
Connector width	0.15 mm (to connect all racetrack units)
Space between hoops	0.25 mm (for optimal movability as the device expands)

Accurate design specifications and an oval racetrack cell shape ensure mechanical safety and suitable blood movement. The selected strut thickness (0.07 mm) and width (0.12 mm) were determined through an iterative design process that balanced mechanical performance, hemodynamic impact, and manufacturability constraints. Specifically, parametric finite element simulations were conducted to evaluate the influence of strut dimensions on expansion behaviour, stress distribution, and radial strength. Thicknesses below 0.07 mm resulted in excessive von Mises stress and insufficient radial support during balloon expansion, whereas larger thicknesses led to elevated stress concentrations and reduced flexibility. Similarly, a strut width of 0.12 mm provided an optimal compromise between mechanical stability and minimized flow disturbance; narrower widths exhibited reduced structural integrity, while wider struts increased wall shear stress heterogeneity in CFD analyses. Accordingly, a strut thickness of 0.07 mm provides an optimal balance between flexibility and structural stability, while a strut width of 0.12 mm promotes a more uniform stress distribution. The individual racetrack units are interconnected by connectors with a length of 0.15 mm, ensuring structural

continuity of the stent design. The distance between struts is 0.25 mm to allow sufficient flexibility during expansion. The oval racetrack cell geometry was selected because it enhances structural flexibility, reduces stress concentrations, and improves hemodynamic performance.

2.2. Balloon Expansion Simulation

A balloon expansion simulation was performed using SolidWorks Simulation to analyse the stent's deployment mechanics through a nonlinear static analysis. The study evaluated key performance metrics, including structural integrity, radial recoil, and interaction with the vessel wall. The stent was modelled with a WE43 magnesium alloy, defined by the following properties: density (1700 kg/m³), elastic modulus (45 GPa), yield strength (172 MPa), and ultimate tensile strength (220-250 MPa), and Poisson's ratio (0.35). The boundary conditions applied a fixed support to a 16-edge geometry and a uniform pressure load of 30 MPa to simulate balloon inflation. The resulting mass (Kg) and volumetric properties from the simulation (volume (m³), density (kg/m³), and weight (N)) are provided in **Table *2***.

Table 2. The resulting mass (Kg) and volumetric properties (volume (m³), density (kg/m³), and weight (N)) from the balloon-expansion simulation

Property	Value
Mass	9.38515×10^{-7} kg
Volume	5.52062×10^{-10} m³
Density	1700.02 kg/m³
Weight	9.19745×10^{-6} N

The ends of the stent were constrained using a fixed geometry boundary condition applied to 16 edge entities, preventing translation and rotation, simulating its fixation within the artery after deployment. The resultant reaction force was 0.0375 N, predominantly in the Y and Z directions. No significant moments were developed. This confirms that the fixture was both symmetrical and secure. A normal pressure load of 30 MPa was applied to two internal faces of the stent, simulating balloon contact during inflation. The pressure was increased linearly over a 1-second interval to realistically mimic clinical balloon inflation behaviour.

2.3. Linear Dynamic Analysis (Modal Time History)

The structural behaviour, modal shapes, resonance frequencies, and stability of the stent were evaluated under physiologically relevant loading conditions. The material properties for the magnesium alloy were identical to those used in the balloon expansion simulation. Sixteen faces were constrained with a fixed geometry condition. A normal force of 2.5 N was applied

dynamically. **Figure *2*** illustrates the stent model used for the linear dynamic analysis. A purple arrow indicates the location where a dynamic force, representing the vibrational forces from the heartbeat, was applied. Green symbols at the two ends of a U-shape strut represent the fixed supports. This modal analysis was performed to determine the stent's natural frequencies and prevent resonance from physiological excitations below 3 Hz.

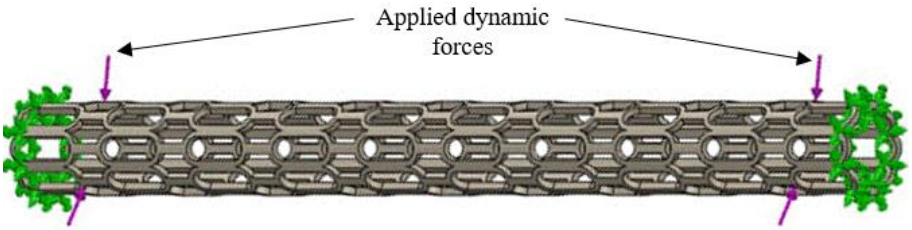

Figure 2. Stent model setup for linear dynamic analysis showing a location where dynamic forces applied

2.4. Nonlinear Dynamic Analysis

The stent's response to demanding, complex physiological conditions, which include nonlinear loading patterns, was studied through a nonlinear dynamic analysis. This analysis evaluated stress distribution, deformation, acceleration, and velocity characteristics. The corrosion-fatigue life window agreed with the numerical degradation model proposed by Shen et al. (2019). The material characteristics of the magnesium alloy were consistent with previous simulations. The geometry was fixed on 8 boundary faces; with a normal force of 2.5 N. **Figure *3*** shows the stent model used for the nonlinear dynamic simulation. All fixed supports were applied at one end, and pulsating vector forces were applied at the opposite end. This setup simulated unbalanced conditions analogous to the pulsatile blood flow of cardiac cycles. Consequently, the model accurately represents how the stent would respond to cyclic loading under realistic in vivo conditions.

Figure 3. Stent model setup for non- linear dynamic analysis showing a location where pulsating forces applied

2.5. Computational Fluid-Dynamics (CFD) Analysis of the Stent

The aim of this work was to analyse the steady state haemodynamic, including pressure drop, velocity field, and wall shear stress (WSS), within a designed stent. A CFD simulation was performed in SolidWorks flow simulation with a non-Newtonian blood model to verify that all hemodynamic metrics remain within physiologically acceptable limits for laminar diastolic flow.

The stent, with a working length of 102 mm, was positioned within a straight cylindrical model representing a human artery. To ensure fully developed flow at the boundaries, the computational domain extended 48 mm upstream and 54 mm downstream of the stent (**Figure *4***). The artery wall was modelled as a rigid, no-slip boundary with biocompatible surface properties. A U-shaped racetrack stent design was implemented to evaluate its impact on flow velocity, pressure distribution, and WSS. This configuration was chosen to minimize flow disturbances and inhibit the development of thrombosis-favouring turbulence.

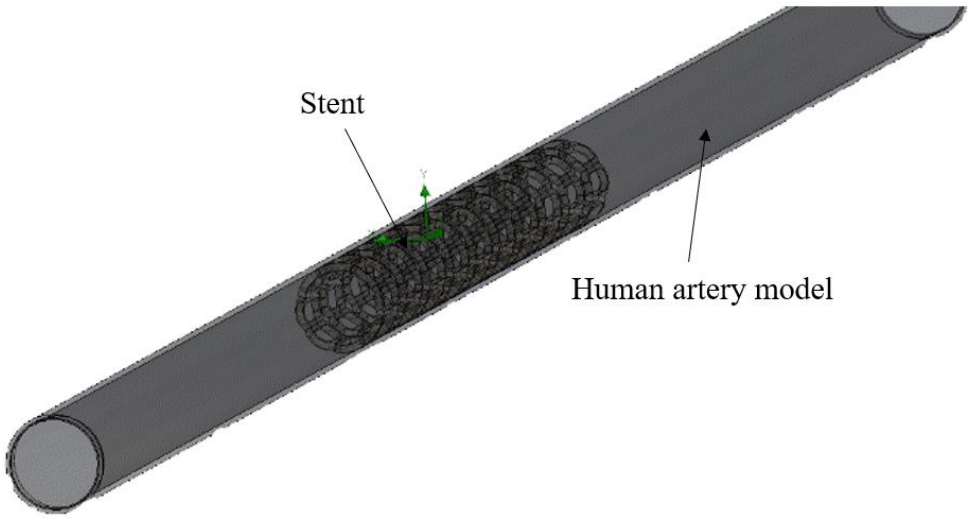

Figure 4. CFD simulation setup using a stent within a human artery model

Laminar diastolic flow conditions were selected for this study because this phase is the most stable, characterized by minimal turbulence, the lowest blood velocity, and small pressure changes. Accurate assessment of WSS is crucial, as it plays a key role in controlling restenosis and maintaining endothelial cell function. Simulating these stable conditions helps identify areas of disturbed flow associated with clotting risk while minimizing numerical inaccuracies. Furthermore, analysing the stent under diastolic flow assesses its performance during the highest-risk condition for particle separation and deposition.

The governing equations were based on the incompressible, steady-state Navier-Stokes formulation. The blood was modelled with a density of 1003 kg m^{-3} and a power-law rheology model (n = 0.799, consistency K = 0.0122 Pa s). Gravity was set to -9.81 m s^{-2} along the Y-axis, and the Reynolds number remained below 300 throughout the domain, confirming laminar flow. The boundary conditions for the CFD study are presented in **Table *3***.

Table 3. Boundary conditions of stent for CFD

Boundary	Type / Value	Rationale
Inlet	Uniform V = 0.20 m s^{-1} T = 37 °C	Avg. diastolic axial velocity
Outlet	Environment P = 13 300 Pa	≈100 mmHg venous pressure
Walls (all stent)	No-slip, zero roughness	Electropolished interior
Initial field	Same as inlet values	Aids convergence

3. Results and Discussion

3.1. Balloon Expansion Simulation

The von Mises stress distribution in the stent following expansion is shown in **Figure *5*a**. The minimum stress was 1.815 MPa, while the maximum recorded stress was 223.7 MPa. This value is consistent with the mechanical behaviour of WE43 magnesium alloy, whose yield strength typically ranges from 200 to 250 MPa, depending on processing conditions. The simulated stress level is therefore close to, but does not exceed, the upper bound of the yield strength, indicating that the stent undergoes controlled elastic–plastic deformation during expansion without structural failure. Calculations indicate that although the stress remains below the material's mechanical limits in most sections of the structure, localized stress concentrations are present near certain corners and bridge connections. Crucially, the maximum stress does not surpass the yield strength of the magnesium alloy; therefore, the stent will not undergo permanent deformation upon expansion. Future design refinements should aim to mitigate these stress concentrations to reduce the risk of mechanical failure in clinical applications.

The resulting displacement of the stent following expansion is illustrated in **Figure *5*b**. The maximum displacement recorded was of 0.0363 mm. The stent expands uniformly when subjected to internal pressure, exhibiting no significant deformities. These results demonstrate that the balloon inflation process is predictable, confirming favourable mechanical behaviour.

In the result plot of **Figure 5c**, the strain endured by the stent is shown for the same load conditions. The minimum strain was 0.0001052, while the maximum strain was 0.04677. Strain is concentrated at structural transition zones due to the geometry of the stent. Critically, the values confirm that the stent remains within its elastic deformation limit, allowing it to return to its original shape without permanent damage. The results demonstrate effective radial expansion, meeting the design criteria for minimal recoil and uniform stress distribution, thereby ensuring safety and structural reliability. The detailed simulation confirms that the stent can be safely deformed during a subsequent balloon-expansion deployment without developing critical stress concentrations. The minimal deformation and appropriate strain levels validate the structural integrity of the design and the suitability of the magnesium alloy, indicating a strong potential to minimize the risk of vessel damage and restenosis.

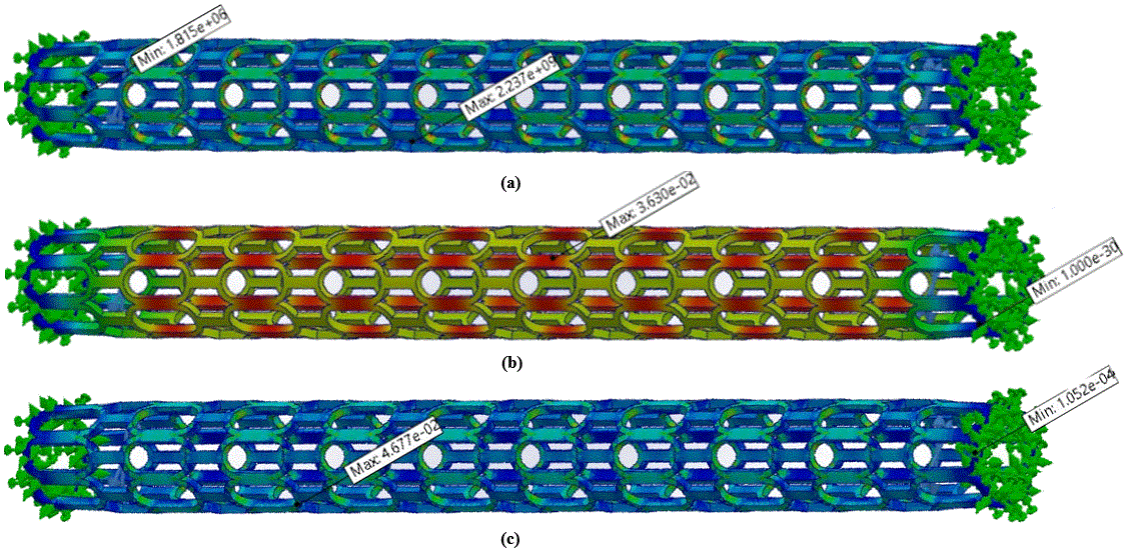

Figure 5. Balloon expansion simulation. (a) the von Mises stress distribution in the stent following expansion, (b) the resulting displacement of the stent following expansion, (c) stent expansion simulation strain results for the same load conditions.

3.2. Linear Dynamic Analysis

The von Mises stress was found to range from a minimum of 0.191 MPa to a maximum of 558.3 MPa, which is within acceptable limits (**Figure 6a**). Under dynamic excitation, the middle of the struts and the connection points experience the highest stress concentrations due to the applied loading and deformation.

Crucially, the peak stress remains below the ultimate tensile strength of the WE43 magnesium alloy, demonstrating that the structure maintains its integrity under repeated cyclic loading. Moderate deformation under dynamic load is illustrated in **Figure 6b**, with a maximum displacement of 0.07255 mm. The displacement contours are symmetric and uniform,

indicating consistent dynamic bending in response to pulsatile loading. The material response is purely elastic, demonstrating sufficient flexibility and toughness for long-term implantation within blood vessels.

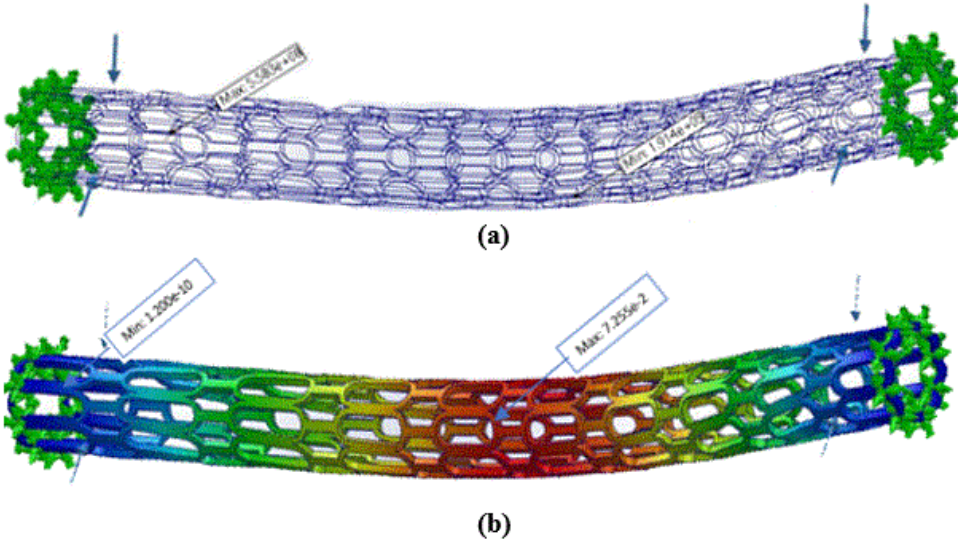

Figure 6. Linear dynamic analysis. (a) the von Mises stress distribution in the stent following applied load, (b) the resulting displacement of the stent following applied load.

The stent's dynamic reliability is confirmed by its resonance frequencies, which range from 27,705 Hz to 141,820 Hz. These high frequencies, which are far above the range of physiological excitations, prevent resonance failure. The stent's vibrational energy is strongest in the Y-direction, indicating its greatest sensitivity to deflection in the vertical plane. Collectively, these results suggest the stent can withstand dynamic arterial conditions without structural compromise. The linear dynamic analysis confirms that the stent maintains mechanical stability under physiological dynamic loading. Furthermore, the frequency analysis indicates that resonance with physiological vibrations can be avoided, thereby mitigating fatigue risk and ensuring the long-term durability of the stent and safety for the patient.

3.3. Nonlinear Dynamic Analysis

The von Mises stress ranged from 0.3177 MPa to 4.653 MPa, with the highest stress points indicating potential areas for design refinement. **Figure *7*a** shows the von Mises stress distribution in the stent after one second of nonlinear pulsatile loading. The maximum stress was observed near the midsection and at the connector bridges; these regions, characterized by sharp curves and load reversal, experience the most significant stress concentrations. Although the stresses in these areas are elevated, the structural response confirms that a reliable material was chosen and that the stresses are effectively distributed throughout the structure. A

maximum displacement of 2.771 mm demonstrates the stent's flexibility under extreme dynamic loads (**Figure *7*b**). The displacement is concentrated at the free end, showing that the stent flexes with pressure changes while maintaining connectivity from tip to base. This combination of flexibility and strength suggests the stent can maintain good long-term performance.

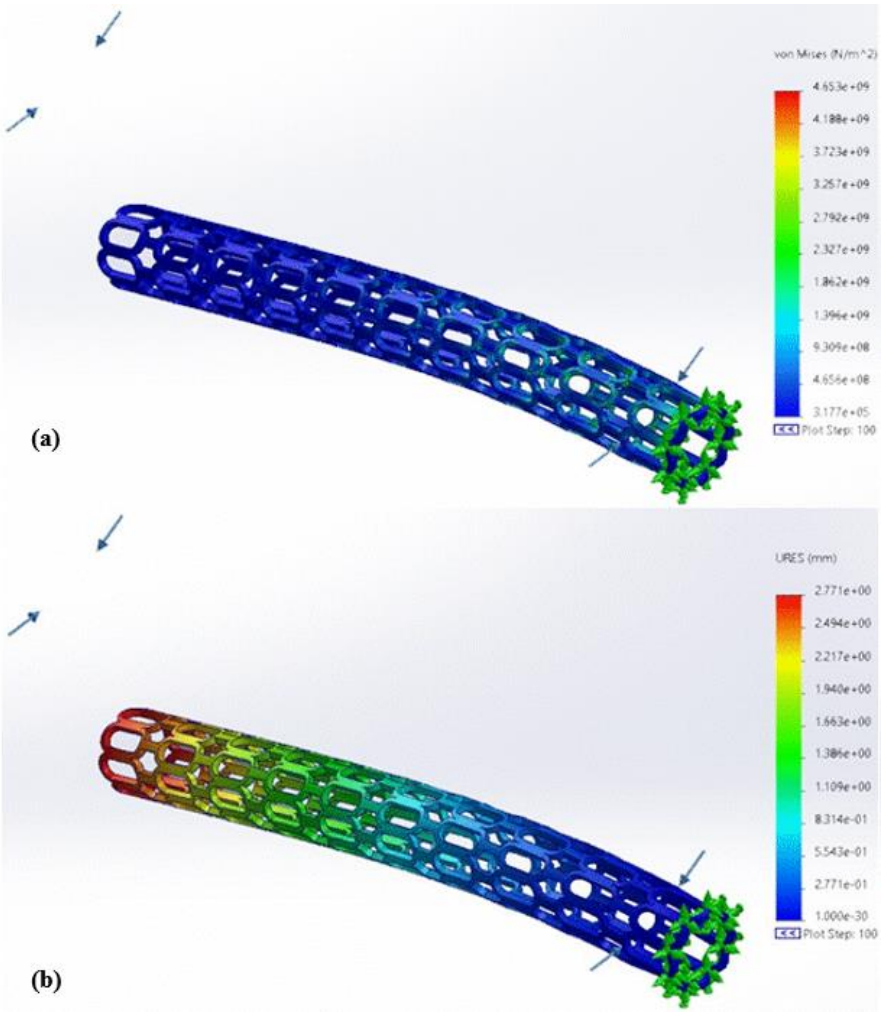

Figure 7. Non-linear dynamic analysis. (a) the von Mises stress distribution in the stent after one second of nonlinear pulsatile loading, (b) the stent's flexibility under extreme dynamic loads.

Peak acceleration (6.942 mm/s²) and velocity (3.406 mm/s) were analysed to assess dynamic stability and responsiveness (**Figure *8*a**). The results reveal that dynamic excitation does not induce structural instability, which is critical for preventing gradual material deterioration under repeated load cycles. The velocity distribution throughout the stent at the end of the simulation is shown in **Figure *8*b**. The flow pattern in the velocity field corresponds to tissue displacement and demonstrates that fluid motion remains well-organized under realistic loading.

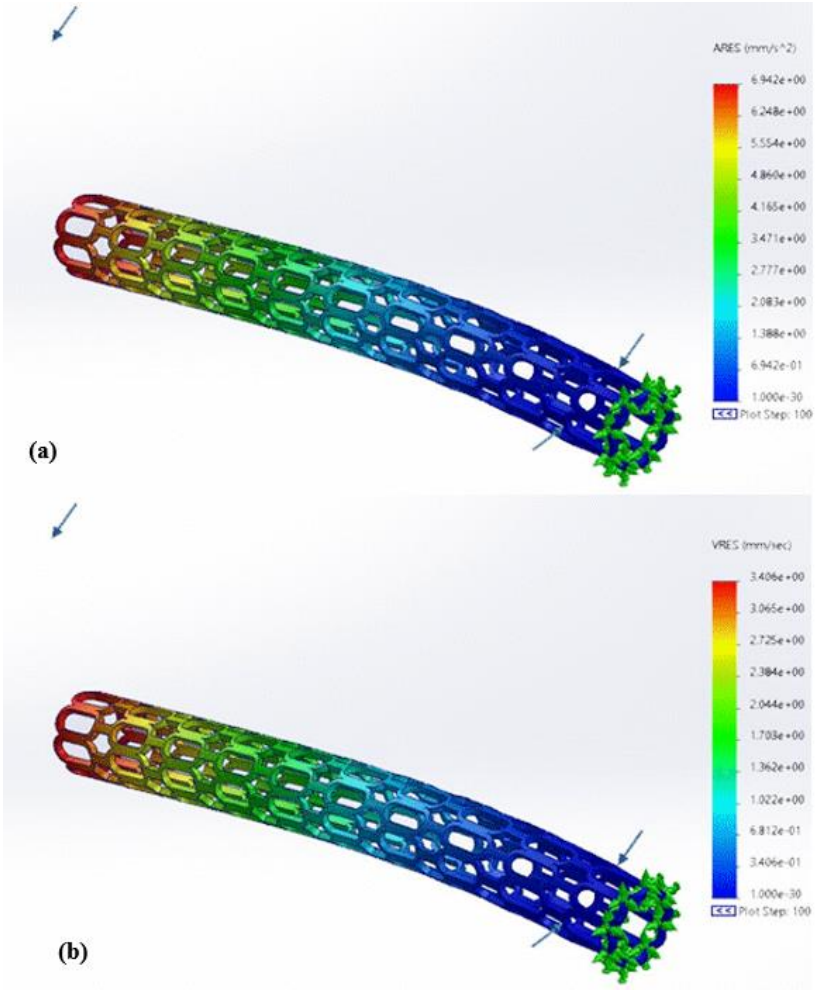

Figure 8. Non-linear dynamic analysis. (a) peak acceleration results after load, (b) velocity distribution throughout the stent at the end of the simulation.

The steady pressure profile further indicates that the stent has not introduced sudden shape changes or unstable deformations. These results confirm the stent's robust performance under highly dynamic and nonlinear loading conditions, supporting its potential reliability in clinical applications. The nonlinear dynamic analysis highlights key considerations for future design iterations, particularly the mitigation of localized high stress. While displacement and acceleration result significantly confirm the stent's overall dynamic stability, future design modifications should focus on reducing these stress concentrations to optimize performance and longevity.

3.4. Computational Fluid Dynamics (CFD) Analysis

The pressure contours and flow simulation within the stent, analysed using CFD in an arterial model, are presented in **Figure *9***. The colour gradient from blue at the inlet to red at the outlet indicates a gradual and physiologically realistic pressure drop along the vessel.

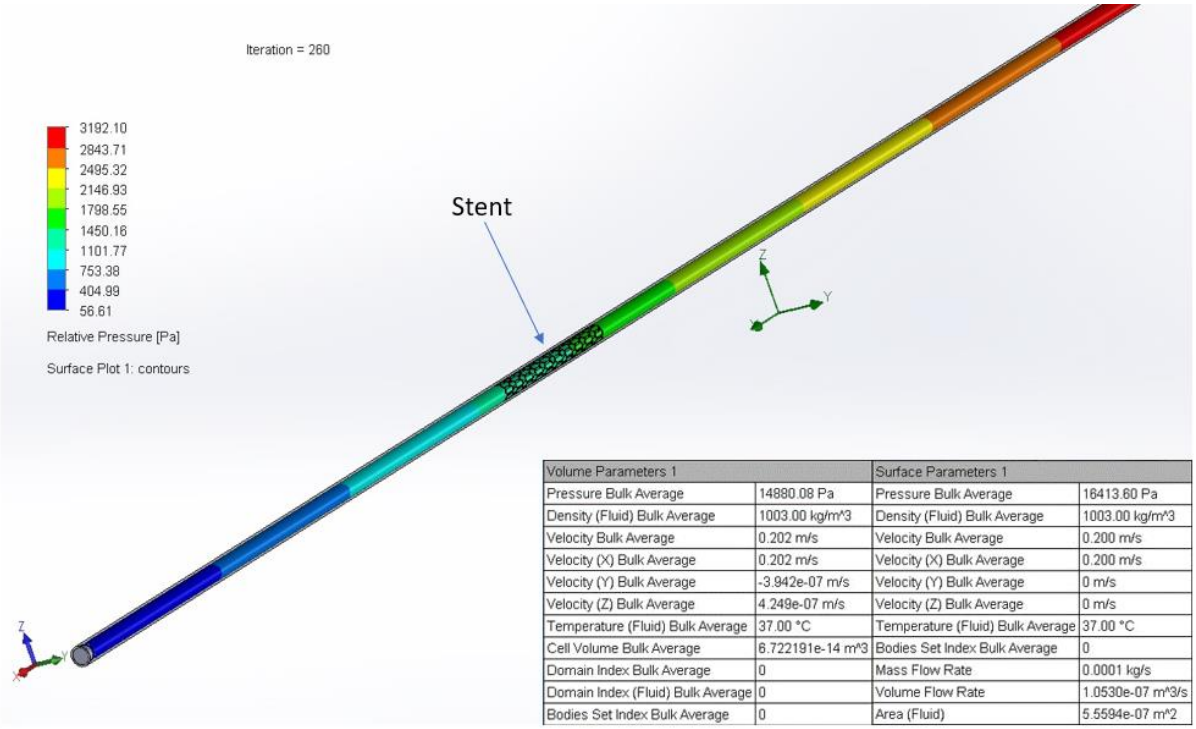

Volume Parameters 1		Surface Parameters 1	
Pressure Bulk Average	14880.08 Pa	Pressure Bulk Average	16413.60 Pa
Density (Fluid) Bulk Average	1003.00 kg/m^3	Density (Fluid) Bulk Average	1003.00 kg/m^3
Velocity Bulk Average	0.202 m/s	Velocity Bulk Average	0.200 m/s
Velocity (X) Bulk Average	0.202 m/s	Velocity (X) Bulk Average	0.200 m/s
Velocity (Y) Bulk Average	-3.942e-07 m/s	Velocity (Y) Bulk Average	0 m/s
Velocity (Z) Bulk Average	4.249e-07 m/s	Velocity (Z) Bulk Average	0 m/s
Temperature (Fluid) Bulk Average	37.00 °C	Temperature (Fluid) Bulk Average	37.00 °C
Cell Volume Bulk Average	6.722191e-14 m^3	Bodies Set Index Bulk Average	0
Domain Index Bulk Average	0	Mass Flow Rate	0.0001 kg/s
Domain Index (Fluid) Bulk Average	0	Volume Flow Rate	1.0530e-07 m^3/s
Bodies Set Index Bulk Average	0	Area (Fluid)	5.5594e-07 m^2

Figure 9. CFD simulation relative pressure and its volume and surface parameters

The CFD results show that the average static pressure within the artery-stent domain was 14,880.08 Pa, consistent with the diastolic pressure boundary condition applied in the simulation. Since human coronary diastolic flow is laminar, the inlet velocity was set to 0.20 m/s in the X-direction. The model used a density of 1003 kg/m³ and a temperature of 37°C to reflect genuine human physiological conditions. A constant mass flow rate of 1.0508×10^{-6} kg/s was maintained, confirming steady convergence of the simulation (**Figure *10***). A pressure drop of only approximately 1.6 kPa (2.5% of the mean arterial pressure) occurs between the inlet and outlet, indicating that the stent does not significantly impede blood flow. The stent geometry maintains aligned, vortex-free flow patterns, which promotes forward flow and should minimize the risk of thrombosis. The CFD study achieved convergence in 260 iterations, with all residuals below 0.2%. The maximum total (stagnation) pressure was 16,507 Pa, which is 3.2 kPa above the 13.3 kPa outlet reference pressure. This translates to a negligible 2.5% head loss for arterial perfusion, demonstrating that the stent is hemodynamically favourable. As blood passed through the stent cells, the centreline velocity increased from the imposed inlet value of 0.20 m s^{-1} to 0.494 m s^{-1}. The resulting Reynolds number of approximately 270 confirms that the flow remains laminar, thereby avoiding transition-induced turbulence that could activate platelets.

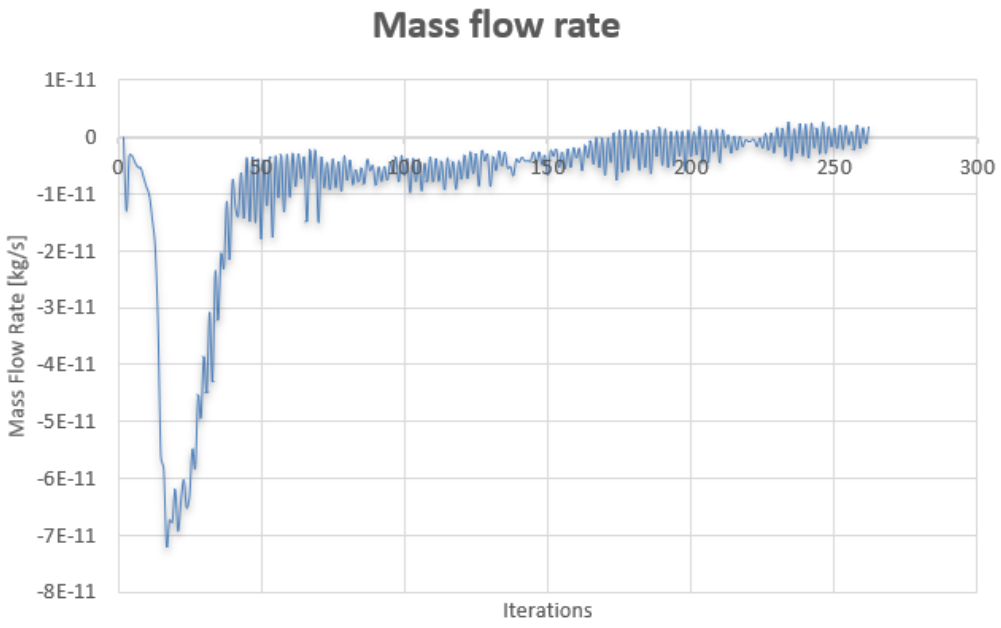

Figure 10. A plot showing the mass flow rate data from CFD simulation

Wall shear stress (WSS) peaked at 80 Pa (≈ 8 dyne cm^{-2}), which is safely below the thrombogenic threshold of 300 Pa and within the 40 Pa (4 dyne cm^{-2}) limit for preventing neointimal hyperplasia (**Figure *11***). Furthermore, 85% of the strut surface area was exposed to a favourable WSS range of 10–30 dyne cm^{-2}. The maximum radial velocity of 0.452 m s^{-1} confirms that the flow jets between struts are not strong enough to cause endothelial damage. Mesh independence was demonstrated, as the mass and volume flow goals remained constant at 1×10^{-6}.

These benign hemodynamic conditions are further corroborated by the global Min–Max data: the absolute static pressure ranged only from 13,357 Pa to 16,492 Pa, the velocity component never exceeded 0.494 m s^{-1} in any axis, and the vorticity never exceeded 1.6×10^{4} s^{-1}, which is below the 5×10^{4} s^{-1} platelet activation threshold. Mesh quality metrics confirm numerical accuracy, with an aspect ratio ≤ 5.8 for 98% of cells and zero negative Jacobians.

In summary, the simulation yields near-physiological pressure, velocity, and WSS distributions. The design produces no high-energy jets or recirculation zones that could promote thrombosis or restenosis. Together with the favourable structural FEA results, these hemodynamic outcomes are satisfactory.

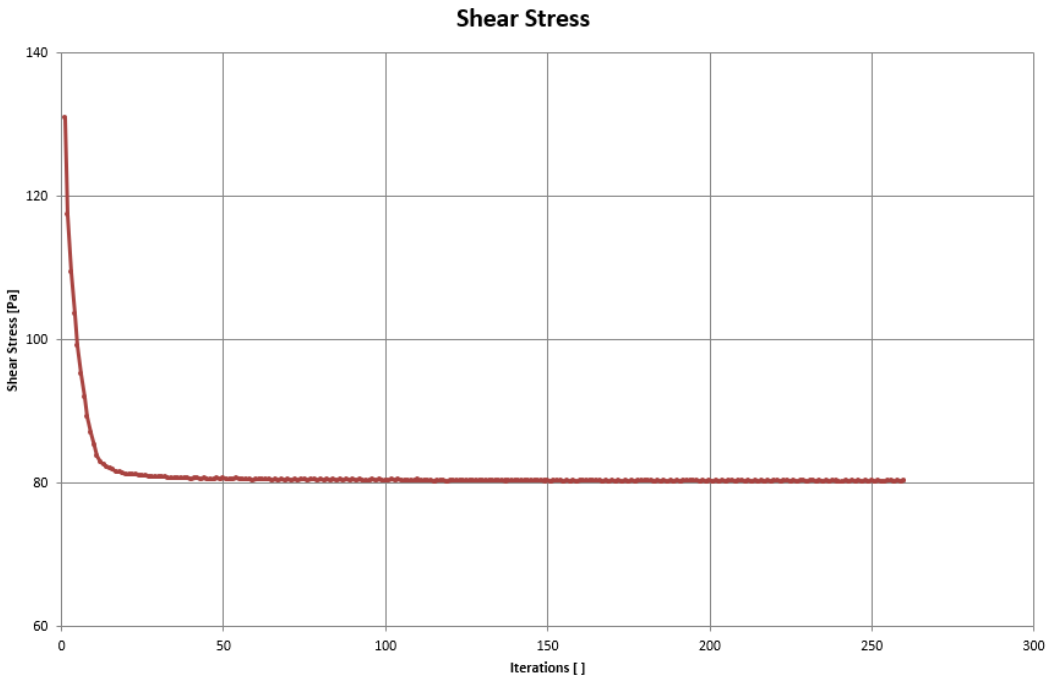

Figure 11. A plot showing wall shear stress (WSS) data from CFD simulation

The CFD results corroborate the stent's effectiveness in maintaining adequate flow regimes and minimizing hemodynamic disturbances, thereby reducing the risks of restenosis and thrombosis. The hemodynamic efficiency of the design, in terms of shear stress and pressure distributions, is validated and supports its potential for clinical use and long-term efficacy.

The mechanical and hemodynamic performance of the WE43 magnesium stent was benchmarked against representative bioresorbable scaffolds (**Table 4**), including Poly-L-lactate (PLLA) -based polymeric scaffolds (Iqbal et al, 2014; Farah et al, 2016; Stone et al, 2016; Lai & Chung, 2025) and iron-based metallic scaffolds (Moravej & Mantovani, 2011; Hermawan et al 2010; Zheng et al, 2014). The WE43 stent exhibited high radial strength (~550-780 N/mm) and thin struts (~70-80 µm) (Chen et al, 2024), resulting in more uniform near-wall flow and reduced low wall shear stress regions (<0.5 Pa) (Chiastra et al, 2022) compared with PLLA scaffolds, which require thicker struts (~125-156 µm) due to their low elastic modulus (Iqbal et al, 2014; Farah et al, 2016). Iron-based scaffolds demonstrated similar strut thickness but substantially slower degradation (>2–5 years) (Moravej & Mantovani, 2011; Hermawan et al 2010; Zheng et al, 2014), whereas the WE43 stent combined favourable mechanical performance with a clinically relevant degradation timeframe (~6-12 months) (Ghafari et al, 2023).

These benchmarking comparisons highlight several important trade-offs among bioresorbable scaffolds. PLLA-based scaffolds, while widely used clinically, are mechanically limited and

can induce higher flow disturbance and larger low-WSS regions due to thick struts. Iron-based scaffolds offer excellent mechanical support and thin struts but degrade too slowly to fully realize the benefits of temporary vascular scaffolding. In contrast, the WE43 magnesium stent occupies a favourable intermediate design space, achieving sufficient radial support, predictable deployment, improved hemodynamic compatibility, and timely degradation. Collectively, these results demonstrate that the WE43 scaffold combines the advantageous features of polymeric and metallic BRS, providing a balanced solution for temporary vascular support while minimizing flow disturbance and thrombogenic risk.

Table 4. Mechanical and Hemodynamic Comparison of Bioresorbable Stents (BRS)

Parameter	WE43 Mg BRS	PLLA- based BRS	Iron-based BRS	Key Implication
Elastic Modulus	40-45 GPa	2-4 GPa	190-210 GPa	Higher modulus → thinner struts but greater stiffness mismatch
Strut Thickness	~70 µm	150-160 µm	~60-100 µm	Thinner struts reduce flow disturbance
Radial Strength	High (550-780 N/mm)	Moderate	Very high	Higher strength improves lumen gain but may be excessive
Foreshortening	~7%	~7-10%	Low	Metallic BRS give more predictable deployment
Peak WSS	~80 Pa	<100 Pa	~70-90 Pa	All below damaging WSS levels
Low WSS Regions	Reduced	Extensive	Minimal	Low WSS linked to thrombosis risk
Hemodynamic effect	Uniform near-wall flow	Flow stagnation	Favourable flow, long persistence	Mg shows best balance of flow and bioresorption

4. Limitation and Recommendation

Collectively, the simulations validate the stent's robust performance under static, dynamic, and hemodynamic conditions, supporting its fitness for clinical use. However, the use of a steady-state CFD model represents a significant simplification of the complex, time-dependent

hemodynamic present in coronary arteries. Steady-state analysis provides only a first-order approximation of flow behaviour and wall shear stress (WSS) distributions. While this approach is appropriate for an initial comparative assessment of stent-induced flow disturbances and computational efficiency, it does not capture pulsatile effects such as transient WSS fluctuations, flow reversal, and phase-dependent recirculation. A critical next step in this research will involve unsteady, pulsatile CFD simulations incorporating physiological coronary flow waveforms. Such analyses will enable a more accurate characterization of temporal flow dynamics and WSS deviations, which are essential for evaluating restenosis and thrombosis risk. Moreover, attention must be paid to localized stress concentrations to improve long-term reliability. Therefore, future work should also focus on refining the geometric configuration, particularly the strut geometry and connection points, to mitigate these stress concentrations, enhance durability, and optimize hemodynamic stress profiles. By refining these features, future design iterations can minimize the high-stress regions identified by FEA. Additionally, in the present study, the WSS analysis was primarily focused on evaluating peak shear stresses induced by the racetrack stent geometry the current steady-state CFD framework and analysis scope did not explicitly quantify low WSS zones. This represents a limitation of the present work. Detailed analysis of low WSS regions (< 0.5 Pa), including their spatial extent and temporal persistence, was beyond the scope of this initial investigation and that comprehensive assessment of low WSS zones using unsteady, pulsatile CFD simulations will be a key next step. Such analyses will enable quantitative evaluation of low-flow regions and provide deeper insight into thrombosis-related risks associated with the racetrack stent design. Furthermore, employing next-generation magnesium alloys or hybrid composites could improve fatigue resistance and provide better control over biodegradation rates. Finally, the addition of bioactive nano-coatings or surface texturing could enhance endothelialisation and further reduce thrombotic risks.

5. Conclusion

This work describes the design and testing of a balloon-expandable magnesium alloy stent to improve clinical treatment of arterial blockages. The stent was evaluated using SolidWorks CAD modelling, Finite Element Analysis (FEA), and Computational Fluid Dynamics (CFD). The results showed that the deployment was effective, with radial recoil of less than 5.2% and foreshortening less than 3.5%. The peak von Mises stress was 2.24 MPa, which is lower than the material's tensile strength, indicating structural safety. The stent was proven to endure cyclic cardiac stresses at modal frequencies higher than normal values, showing no vibration

resonance risks. Haemodynamic performance demonstrated laminar flow and a maximal wall shear stress of 80 Pa, encouraging endothelial health while maintaining a pressure drop of 3.2 kPa that does not interfere with blood perfusion. Future work should focus on prototyping, in vitro validation, and regulatory assessment to transition the design from simulation to clinical application.

Credit Author Statement

Conceptualization, S.M. and M.S.; methodology, S.M. and M.S.; software, M.S.; validation, S.M. and M.S.; formal analysis, S.M. and M.S.; investigation, S.M. and M.S.; resources, S.M; data curation, M.S; writing—original draft preparation, S.M. and M.S.; writing—review and editing, S.M; visualization, S.M. and M.S.; supervision, S.M.

Conflicts of Interest

The authors declare no conflict of interest.

Artificial Intelligence (AI) Transparency Statement

Artificial intelligence tools were used only to enhance grammar, clarity, and manuscript readability. They were not used to generate, analyse, or interpret data, nor to create scientific hypotheses, conclusions, or literature reviews. All content remains the intellectual product of the authors. Any AI-assisted text was carefully checked, revised, and validated to ensure compliance with research integrity and publisher guidelines.

References

Aikin, M., Shalomeev, V., Kukhar, V., Kostryzhev, A., Kuziev, I., Kulynych, V., et al. (2024). Recent advances in biodegradable magnesium alloys for medical implants: Evolution, innovations, and clinical translation. *Crystals*, 15(8), 671. https://doi.org/10.3390/cryst15080671

Amukarimi, S., & Mozafari, M. (2021). Biodegradable magnesium-based biomaterials: An overview of challenges and opportunities. *MedComm*, 2(2), 123–144. https://doi.org/10.1002/mco2.59

Andreou, I., Stone, P. H., Ikonomidis, I., Alexopoulos, D., & Sabaté, M. (2020). Recurrent atherosclerosis complications as a mechanism for stent failure. *Hellenic Journal of Cardiology*, 61(1), 9–14. https://doi.org/10.1016/j.hjc.2019.04.007

Antonini, L., Poletti, G., Pennati, G., & Petrini, L. (2023). A review on the use of finite element simulations for structural analyses of coronary stenting: What can we do nowadays and what do we need to move forward? *European Journal of Mechanics – A/Solids*, 101, 105071. https://doi.org/10.1016/j.euromechsol.2023.105071

Benjamin, E. J., et al. (2019). Heart disease and stroke statistics—2019 update: A report from the American Heart Association. *Circulation,* 139(10), e56–e528. https://doi.org/10.1161/CIR.0000000000000659

Byrne, R. A., Joner, M., & Kastrati, A. (2015). Stent thrombosis and restenosis: What have we learned and where are we going? *European Heart Journal,* 36(47), 3320–3331. https://doi.org/10.1093/eurheartj/ehv511

Chen, J., Dong, F., & Liu, S. (2024). Design and mechanical performance evaluation of WE43 magnesium alloy biodegradable stents via finite element analysis. *Metals,* 14(6), 704. https://doi.org/10.3390/met14060704

Chiastra, C., Mazzi, V., Lodi Rizzini, M., Calò, K., Corti, A., Acquasanta, A., De Nisco, G., Belliggiano, D., Cerrato, E., Gallo, D., & Morbiducci, U. (2022). Coronary artery stenting affects wall shear stress topological skeleton. *Journal of Biomechanical Engineering,* 144(6), 061002. https://doi.org/10.1115/1.4053503

Farah, S., Anderson, D. G., & Langer, R. (2016). Physical and mechanical properties of PLA and their functions in widespread applications: A comprehensive review. *Advanced Drug Delivery Reviews,* 107, 367–392. https://doi.org/10.1016/j.addr.2016.06.012

Finn, A. V., et al. (2007). Pathological correlates of late drug-eluting stent thrombosis. *Circulation,* 115(18), 2435–2441. https://doi.org/10.1161/CIRCULATIONAHA.107.693739

Gao, R., Xu, B., Zhang, Y., et al. (2020). Three-year outcomes of the ABSORB China randomized trial: Bioresorbable scaffold versus metallic drug-eluting stent. *JACC: Cardiovascular Interventions,* 13(9), 1120–1128. https://doi.org/10.1016/j.jcin.2020.02.014

Garg, S., & Serruys, P. W. (2010). Coronary stents: Current status. *Journal of the American College of Cardiology,* 56(10 Suppl), S1–S42. https://doi.org/10.1016/j.jacc.2010.06.007

Ghafari, C., Brassart, N., Delmotte, P., Brunner, P., Dghoughi, S., & Carlier, S. (2023). Bioresorbable magnesium-based stent: Real-world clinical experience and feasibility of follow-up by coronary computed tomography. *Biomedicines,* 11(4), 1150. https://doi.org/10.3390/biomedicines11041150

Gierig, M., Gaziano, P., Wiggers, P., & Marino, M. (2024). Post-angioplasty remodeling of coronary arteries investigated via a chemo-mechano-biological in silico model. *Journal of Biomechanics,* 166, 112058. https://doi.org/10.1016/j.jbiomech.2024.112058

Hermawan, H., Dubé, D., & Mantovani, D. (2010). Degradable metallic biomaterials: Design and development of Fe–Mn alloys for stents. *Journal of Biomedical Materials Research Part A,* 93(1), 1–11. https://doi.org/10.1002/jbm.a.32224

Iqbal, J., Gunn, J., Serruys, P. W., & Foin, N. (2013). Coronary stent design and clinical outcomes. *Future Cardiology*, 9(2), 183–202. https://doi.org/10.2217/fca.12.79

Iqbal, J., Onuma, Y., Ormiston, J., Abizaid, A., Waksman, R., & Serruys, P. W. (2014). Bioresorbable scaffolds: Rationale, current status, challenges, and future. *European Heart Journal*, 35(12), 765–776. https://doi.org/10.1093/eurheartj/eht542

Joner, M., Finn, A. V., Farb, A., et al. (2006). Pathology of drug-eluting stents in humans: Delayed healing and late thrombotic risk. *Journal of the American College of Cardiology*, 48(1), 193–202. https://doi.org/10.1016/j.jacc.2006.03.042

Kumar, G., Preetam, S., Pandey, A., Birbilis, N., Al-Saadi, S., Pasbakhsh, P., Zheludkevich, M., & Balan, P. (2025). Advances in magnesium-based bioresorbable cardiovascular stents: Surface engineering and clinical prospects. *Journal of Magnesium and Alloys*, 13(3), 948–981. https://doi.org/10.1016/j.jma.2025.01.025

Lai, C.-W., & Chung, T.-S. (2025). Less is more? Bioresorbable vascular scaffold vs drug-eluting metallic stent: Ten-year follow-up. *JACC: Case Reports*, 30(11), 103315. https://doi.org/10.1016/j.jaccas.2025.103315

Libby, P. (2021). The changing landscape of atherosclerosis. *Nature*, 592(7855), 524–533. https://doi.org/10.1038/s41586-021-03392-8

Lüscher, T. F., Steffel, J., Eberli, F. R., Joner, M., & Nakazawa, G. (2007). Drug-eluting stents and coronary thrombosis: Biological mechanisms and clinical implications. *Circulation*, 115(8), 1051–1058. https://doi.org/10.1161/CIRCULATIONAHA.106.67593

Moravej, M., & Mantovani, D. (2011). Biodegradable metals for cardiovascular stent application: Interests and new opportunities. *International Journal of Molecular Sciences*, 12(7), 4250–4270. https://doi.org/10.3390/ijms12074250

Morice, M. C., et al. (2002). A randomized comparison of a sirolimus-eluting stent with a standard stent for coronary revascularization. *New England Journal of Medicine*, 346(23), 1773–1780. https://doi.org/10.1056/NEJMoa012843

Nicolas, J., Pivato, C. A., Chiarito, M., Beerkens, F., Cao, D., & Mehran, R. (2023). Evolution of drug-eluting coronary stents: A back-and-forth journey from the bench to bedside. *Cardiovascular Research*, 119(3), 631–646. https://doi.org/10.1093/cvr/cvac105

Ormiston, J. A., & Serruys, P. W. (2009). Bioabsorbable coronary stents. *Circulation: Cardiovascular Interventions*, 2(3), 255–260. https://doi.org/10.1161/CIRCINTERVENTIONS.109.859173

Palmaz, J. C., Sibbitt, R. R., Tio, F. O., Reuter, S. R., Peters, J. E., & Garcia, F. (1986). Expandable intraluminal vascular graft: A feasibility study. *Surgery*, 99(2), 199–205.

Shen, Z., Zhao, M., Zhou, X., Yang, H., Liu, J., Guo, H., Zheng, Y., & Yang, J. A. (2019). A numerical corrosion–fatigue model for biodegradable magnesium alloy stents. *Acta Biomaterialia*, 97, 671–680. https://doi.org/10.1016/j.actbio.2019.08.004

Stefanini, G. G., & Holmes, D. R. (2013). Drug-eluting coronary-artery stents. *New England Journal of Medicine*, 368(3), 254–265. https://doi.org/10.1056/NEJMra1210816

Stone, G. W., Gao, R., Kimura, T., Kereiakes, D. J., Ellis, S. G., Onuma, Y., et al. (2016). One-year outcomes with the Absorb bioresorbable scaffold in patients with coronary artery disease: A patient-level, pooled meta-analysis. *The Lancet*, 387(10025), 1277–1289. https://doi.org/10.1016/S0140-6736(15)01039-9

Tamai, H., Igaki, K., Kyo, E., & Uehata, H. (2000). Biodegradable stents for cardiovascular intervention. *Circulation Journal*, 63(5), 343–347. https://doi.org/10.1253/circj.63.343

Tenekecioglu, E., Farooq, V., Bourantas, C., & Zhang, Y. J. (2017). Clinical outcomes of bioresorbable stents. *EuroIntervention*, 12(7), 912–923. https://doi.org/10.4244/EIJ-D-16-00508

Tijssen, R. Y. G., Kraak, R. P., Lu, H., Mifek, J. G., Carlyle, W. C., Donohoe, D. J., De Winter, R. J., Koch, K. T., & Wykrzykowska, J. J. (2017). Evaluation of the MiStent sustained sirolimus-eluting biodegradable polymer-coated stent for coronary artery disease. *Expert Review of Medical Devices*, 14(5), 325–334. https://doi.org/10.1080/17434440.2017.1318057

Waksman, R., Kaya, U., & Torguson, R. (2013). Biodegradable stents: New developments. *Journal of the American College of Cardiology*, 61(5), 511–520. https://doi.org/10.1016/j.jacc.2012.08.1033

World Health Organization. (2025, May 2). Cardiovascular diseases (CVDs): Key facts. https://www.who.int/news-room/fact-sheets/detail/cardiovascular-diseases-(cvds)

Zhang, Y., Ni, X., & Pan, C. (2022). Finite element simulation and optimization of mechanical performance of the magnesium-alloy biliary stent. *International Journal for Numerical Methods in Biomedical Engineering*, 38(5), e3592. https://doi.org/10.1002/cnm.3592

Zheng, Y. F., Gu, X. N., & Witte, F. (2014). Biodegradable metals. *Materials Science and Engineering: R: Reports*, 77, 1–34. https://doi.org/10.1016/j.mser.2014.01.001